Acta Pharmaceutica Sinica B 2023;13(1):256–270

Chinese Pharmaceutical Association
Institute of Materia Medica, Chinese Academy of Medical Sciences

Acta Pharmaceutica Sinica B

www.elsevier.com/locate/apsb
www.sciencedirect.com

ORIGINAL ARTICLE

Late-stage cascade of oxidation reactions during the biosynthesis of oxalicine B in *Penicillium oxalicum*

Tao Zhang[a,†], Guowei Gu[a,†], Guodong Liu[b], Jinhua Su[c], Zhilai Zhan[d], Jianyuan Zhao[a], Jinxiu Qian[d], Guowei Cai[a], Shan Cen[a], Dewu Zhang[a,*], Liyan Yu[a,*]

[a]*Institute of Medicinal Biotechnology, Chinese Academy of Medical Sciences and Peking Union Medical College, Beijing 100050, China*
[b]*State Key Laboratory of Microbial Technology, National Glycoengineering Research Center, Shandong University, Qingdao 266237, China*
[c]*The Third Medical Center, The General Hospital of People's Liberation Army, Beijing 100039, China*
[d]*National Resource Center for Chinese Materia Medica, China Academy of Chinese Medical Sciences, Beijing 100700, China*

Received 3 August 2022; received in revised form 1 September 2022; accepted 1 September 2022

KEY WORDS

Oxalicine B;
Meroterpenoid;
Biosynthesis;
Cytochrome P450;
Anti-IAV activity

Abstract Oxalicine B (**1**) is an α-pyrone meroterpenoid with a unique bispirocyclic ring system derived from *Penicillium oxalicum*. The biosynthetic pathway of 15-deoxyoxalicine B (**4**) was preliminarily reported in *Penicillium canescens*, however, the genetic base and biochemical characterization of tailoring reactions for oxalicine B (**1**) has remained enigmatic. In this study, we characterized three oxygenases from the metabolic pathway of oxalicine B (**1**), including a cytochrome P450 hydroxylase OxaL, a hydroxylating Fe(II)/α-KG-dependent dioxygenase OxaK, and a multifunctional cytochrome P450 OxaB. Intriguingly, OxaK can catalyze various multicyclic intermediates or shunt products of oxalicines with impressive substrate promiscuity. OxaB was further proven *via* biochemical assays to have the ability to convert 15-hydroxdecaturin A (**3**) to **1** with a spiro-lactone core skeleton through oxidative rearrangement. We also solved the mystery of OxaL that controls C-15 hydroxylation. Chemical investigation of the wild-type strain and deletants enabled us to identify 10 metabolites including three new compounds, and the isolated compounds displayed potent anti-influenza A virus bioactivities exhibiting IC_{50} values in the range of 4.0–19.9 μmol/L. Our studies have allowed us to propose a late-stage

*Corresponding authors. Tel./fax: +86 10 63187118.
E-mail addresses: zhangdewuever@163.com (Dewu Zhang), yly@cpcc.ac.cn (Liyan Yu).
[†]These authors made equal contributions to this work.
Peer review under responsibility of Chinese Pharmaceutical Association and Institute of Materia Medica, Chinese Academy of Medical Sciences.

https://doi.org/10.1016/j.apsb.2022.09.008

biosynthetic pathway for oxalicine B (**1**) and create downstream derivatizations of oxalicines by employing enzymatic strategies.

1. Introduction

Fungal meroterpenoids comprise a unique family of natural products (NPs) partially originating from terpene metabolic pathways that possess remarkable pharmaceutical value due to their complex architectures and bioactivities[1−3]. Biosynthetically, most fungal meroterpenoids are derived from both terpene and polyketide pathways, and these compounds have provided clinical medicinal drugs, such as mycophenolic acid, as well as several promising drug candidates[2,4,5]. The characterization of the biosynthetic gene cluster (BGC) *pyr* of meroterpenoid pyripyropene A accelerated biosynthetic studies on this family of NPs, which have solved many mysteries and elucidated diverse arrays of fascinating enzymes[6−9]. Recently, the biosynthesis of fungal meroterpenoids has attracted increasing interest, as exemplified by austinol[10,11], andrastin A[12,13], yanuthone D[14,15], 15-deoxyoxalicine B[16], terretonin[17−19], anditomin[20], novofumigatonin[21−23], paraherquonin[24,25], and chrodrimanin B[26]. These reports investigated the molecular mechanisms for the synthesis of these compounds and indicated that oxidative enzymes are the key factors responsible for their architectural complexification[1,27]. However, many biosynthetic reactions require further investigation.

Structural diversification in fungal meroterpenoid biosynthesis is usually achieved by transforming a common biosynthetic precursor into various molecules, often with the aid of oxygenases[1,9,27]. Distinct chemical transformation steps often involve cytochrome P450 monooxygenases (P450s) and nonheme iron/α-ketoglutarate (Fe(II)/α-KG)-dependent dioxygenases, which are commonly utilized in biosynthetic pathways of fungal NPs. These enzymes exert a crucial role in the formation of complex structures, including hydroxylation through activating C−H bonds[28], epoxidation[16], dehydrogenation[10,11], C−C bond formation[29,30], C−N coupling[31], carbonate-forming reactions[32], and oxidative skeletal rearrangement[11,17,20,25,33]. Considering the pivotal roles of these P450s or α-KG-dependent oxygenases during biosynthetic processes, the identification of novel oxygenases from nature is of fundamental scientific importance and provides strategies for metabolic engineering of biosynthetic pathways to generate novel compounds for drug development[34].

Oxalicines are naturally occurring α-pyrone meroterpenes[35]. Many α-pyrone meroterpenoids, such as decaturins, exhibit strong antiinsectan activities against *Spodoptera frugiperda*[36,37], and pyripyropenes and arisugacins isolated from the Eurotiaceae family are efficient inhibitors of cholesterol acetylcholinesterase (ACAT) and acetylcholinesterase (AChE), respectively[38,39]. Importantly, biosynthetic elucidation of oxalicines assuredly contributes to clarifying the metabolic process underlying the synthesis of these compounds. The genetic and biosynthetic mechanisms of 15-deoxyoxalicine B (**4**) in *Penicillium canescens* have been investigated by characterization of the biosynthetic gene cluster *olc*, targeted gene disruptions, and bioinformatics analysis[16]. The metabolic pathway up to decaturin C (**5**), the first hemiacetal on-pathway intermediate, was illustrated through gene disruptions. The transformation of hemiacetal intermediate **5** into **4** has also been presented, which is presumably accomplished by three enzymes, including a hydroxylase (OlcK), a predicted transporter (OlcL), and a P450 monooxygenase (OlcB)[16]. However, the biochemical process for the conversion of **5** into oxalicine B (**1**) has not yet been elucidated. Oxalicine B (**1**) is a substantially oxidized diterpenic meroterpene isolated from *P. oxalicum*, *Penicillium thersii*, and *Aspergillus fumigatus* and possesses a rare bispiranic ring and unique hexacyclic ring skeleton[36,37,40-42]. Compared to other meroditerpenes, oxalicine B (**1**) exhibits a wealth of redox modifications. Therefore, understanding the biosynthesis of **1** might provide important new insights into how nature establishes structural complexity initiating from simple precursors (Fig. 1).

In this report, we identified the biosynthetic gene cluster *oxa* for oxalicine B (**1**) in *P. oxalicum*. Using a combination of genetic deletions, chemical complementation, and *in vitro* biochemical reactions, we characterized the required oxygenases in this pathway responsible for the late-stage generation of **1** and on-pathway intermediates. Intriguingly, we confirmed that *oxaL* encodes a cytochrome P450 involved in the hydroxylation of C-15. Another significant finding is the functional characterization of Fe(II)/α-KG-dependent dioxygenase OxaK as a C-23 hydroxylase that exhibits impressive substrate promiscuity. Our analyses also revealed that cytochrome P450 OxaB can generate the spirolactone core skeleton of **1** through oxidative rearrangement. A late-stage biosynthetic pathway from hemiketal decaturin C (**5**) to oxalicine B (**1**) was also proposed. Markedly, the isolated compounds from the deletants exhibited strong anti-influenza A virus (IAV) activities.

2. Results

2.1. Mining and identification of the oxa gene cluster in P. oxalicum 114-2

We examined the fungal genomic sequences available in the NCBI database (https://www.ncbi.nlm.nih.gov/) to obtain the genetic locus potentially participating in the biosynthesis of oxalicine B (**1**). Bioinformatic analysis using the antiSMASH database revealed one cluster in *P. oxalicum* 114-2[43], which was somewhat similar to the biosynthetic gene cluster of 15-deoxyoxalicine B (**4**) (*olc*) in *P. canescens* ATCC 10419 and designated *oxa* (Fig. 2A and Supporting Information Table S2). Based on DNA sequence analysis, an adjacent 27.7 kb *oxa* gene cluster consisting of 12 putative open reading frames (*oxaA*−*oxaM*) was obtained, which might govern the biosynthesis of oxalicine B (**1**). The *oxa* cluster encodes all homologous proteins required for the biosynthetic pathway of compound 15-deoxyoxalicine B (**4**), which is the

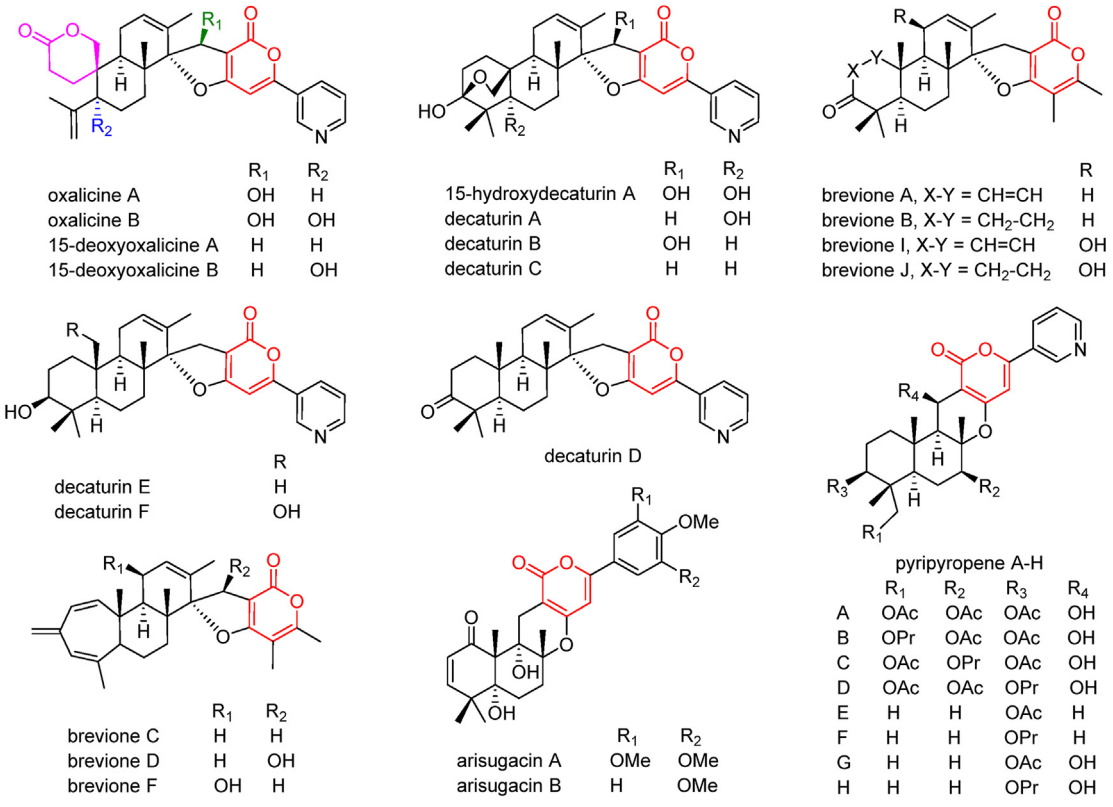

Figure 1 Naturally occurring α-pyrone meroterpenoids. The α-pyrone polyketide unit is in red.

biosynthetic intermediate in the oxalicine B (**1**) pathway. The gene *oxaA* encodes the iterative by partially reducing (PR) PKS OxaA, and Pfam analysis suggested that PKS possesses the domain architecture KS-MAT-DH-MT-KR-ACP, as determined by in silico analysis. Protein BLAST alignment showed that OxaA shares 42% identity to polyketide synthase OlcA (ID: 400488) in *P. canescens* ATCC 10419, 38% identity to Pyr2 (accession no. XP_751268), and a characterized fungal iterative PKS from *A. fumigatus* Af293 functioning in pyripyropene pathway, which are members of the fungal α-pyrone meroterpenoid PKS family (Fig. 1).

Further bioinformatic analysis of the bilateral sequences of the PKS gene enabled the discovery of other genes encoding characteristic enzymes required for meroterpenoid formation. One gene product named OxaI shares greater than 45% amino acid sequence identity with nicotinic acid-CoA ligases, including OlcI and Pyr1, and the latter two enzymes function in the biosynthesis of 15-deoxyoxaciline B (**4**) and pyripyropene, respectively. The gene cluster also encodes the geranylgeranyl pyrophosphate synthase OxaC, the UbiA-like polyprenyl transferase OxaH, FAD-dependent monooxygenase OxaE, and terpene cyclase OxaD, which are probably responsible for the upstream biosynthetic pathway of **1**. Furthermore, four cytochrome P450s (OxaB, OxaG, OxaJ, and OxaL), one Fe(II)/α-KG-dependent dioxygenase (OxaK), and one short-chain dehydrogenase/reductase (SDR, OxaF) encoded by the *oxa* gene cluster are expected to be involved in tailoring modifications and engaged in late-stage biosynthetic pathway. Intriguingly, OxaL exhibits greater amino acid sequence identity (89%) with the uncharacterized cytochrome P450 PaxP in *Penicillium rolfsii* F1880 and shows relatively lower identity (33%) with the biochemically characterized homolog LnaD (ferulate-5-hydroxylase), which is involved in the biosynthesis of diastereomeric piperazinomycin. Our best efforts failed to mine the protein homologous to the P450 OxaL in the *olc* cluster of *P. canescens* ATCC 10419. A detailed analysis of the chemical structures of **1** and **4** showed that **1** contains one more hydroxyl moiety at C-15, suggesting that the enzyme OxaL might catalyze the incorporation of a hydroxyl group at C-15 during oxalicine B (**1**) biosynthesis. Based on the multiple sequence alignments of *oxa* and other meroterpenoid BGCs, we speculated that the *oxa* gene cluster was responsible for producing **1**. Moreover, reverse transcription polymerase chain reaction (rt-PCR) detection also indicated that transcription of the *oxa* family genes is synchronous with the formation of **1** in *P. oxalicum* 114-2 (Supporting Information Fig. S1).

2.2. *Gene deletion studies and characterization of intermediates or shunt metabolites*

P. oxalicum was cultured in MEPA fermentation medium and produced the target α-pyrone-derived meroterpene oxalicine B (**1**) (Fig. 2B, traces v and vi, Fig. 3). Knockout of the *oxaA* gene completely abolished the biosynthesis of **1**, thereby setting up the linkage between the *oxa* cluster and the production of **1** (Fig. 2B, trace iv). We individually deleted three genes, *oxaB*, *oxaL*, and *oxaK* to investigate the biosynthesis pathway and determine the roles of late-stage oxygenases. Compared to the parental strain, the metabolic profiles of Δ*oxaL*, Δ*oxaK*, and Δ*oxaB* exhibited complete abolishment of the formation of compound **1**, and new peaks accumulated and were observed (Fig. 2B, traces i, ii, and iii). The deletant strain Δ*oxaB* was subjected to large-scale fermentation, and the most prominent compound **3** was isolated and purified using column chromatography and semipreparative HPLC. Based on analyses of ^{1}H, ^{13}C, 2D NMR, and MS data, target compound **3** was determined to be 15-hydroxdecaturin A, in

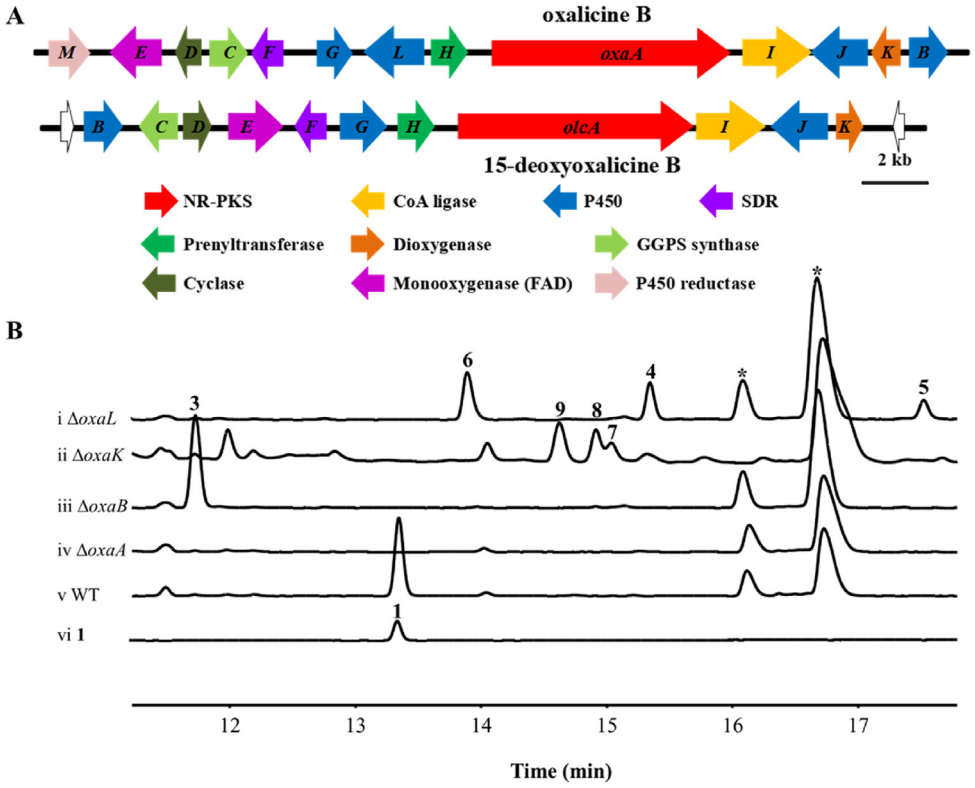

Figure 2 Biosynthetic gene cluster *oxa*, HPLC profiles of the wild-type strain and deletants. (A) Genetic organization of the two gene clusters including *oxa* from *P. oxalicum* and *olc* from *P. canescens*. (B) HPLC analysis of metabolite profiles obtained from the parental strain and deletants (Δ*oxaA*, Δ*oxaB*, Δ*oxaK*, and Δ*oxaL*) of *P. oxalicum*. The organic extracts of strains were discerned by measuring UV absorbance spectra at 310 nm. *These compounds were identified as secalonic acid D and its derivatives.

contrast to the on-pathway intermediate decaturin A (**6**) in 15-deoxyoxalicine B (**4**) biosynthesis reported by Yaegashi and co-workers[7]. The generation of **3** indicated that cytochrome P450 encoded by *oxaB* catalyzes the oxidative rearrangement in the biosynthesis of **1**.

The deletant strain Δ*oxaL* was detected for the formation of new molecules that might denote on-pathway intermediates or shunt products during biosynthesis of oxalicine B (**1**). One oxalicine (**4**) and five decaturin analogs (**5**–**7**, **10**, and **11**) were isolated from the *oxaL* deletant (Fig. 2B, trace i, Fig. 3). Among them, three major compounds were identified as 15-deoxyoxalicine B (**4**)[37], decaturin C (**5**)[36], and decaturin A (**6**)[37] by examining their NMR and MS data with previously presented spectra, which were both intermediates produced during the biosynthesis of **1**. Three minor compounds, including two new decaturin derivatives (**10** and **11**), were determined to be decaturin F (**7**)[44], decaturin H (**10**) and decaturin I (**11**) by analyzing NMR and MS data. Compound **7** was an intermediate in the biosynthesis of **1**, and compounds **10** and **11** might be shunt products. Structurally, these six compounds possessed no hydroxyl group at C-15, suggesting that C-15 hydroxylation was catalyzed by the enzyme encoded by *oxaL*.

Compound **10** possessed an HRESIMS ion peak with *m/z* 504.2369 $[M+H]^+$, corresponding to the molecular formula of $C_{30}H_{33}NO_6$ with 15 degrees of unsaturation. The ^1H and ^{13}C NMR spectra of **10** were similar to those of decaturin C (**5**). The obvious difference includes the presence of a carbonyl moiety (δ_C 173.5) in **10** instead of an oxygenated methylene group [δ_H 4.22 (1H, dd, J = 9.0, 3.0 Hz), 3.91 (1H, dd, J = 9.0, 1.8 Hz); δ_C 67.8] in **5** (Supporting Information Figs. S16 and S17). The location of the carbonyl moiety was further confirmed by the HMBC correlations of H-19, H-23, and H-25 with C-29. A detailed analysis of DEPT, $^1H-^1H$ COSY, HSQC, and HMBC spectra established the complete assignment of **10**. The stereochemistry of **10** was proposed to be the same as those of **5** by analyzing ^1H and ^{13}C NMR data, NOESY correlations, ECD spectra, and biogenic pathways. Taken together, compound **10** might not be the precursor of oxalicine B (**1**), but is clearly an off-pathway product.

Compound **11** exhibited a quasi-molecular ion $[M+H]^+$ at *m/z* 518.2528 in its HRESIMS spectrum, consistent with the molecular formula of $C_{31}H_{35}NO_6$, suggesting that a methyl moiety may be introduced compared with **10**. The ^1H and ^{13}C NMR spectra (Supporting Information Table S4) for **11** resembled those of **10**, except for the presence of a methoxy moiety (δ_H 3.30; δ_C 50.5). The HMBC correlation from H_3-34 to C-27 confirmed the position of the methoxy group. The stereochemistry of **11** was proposed to be analogous to that of **10** based on the NMR data, NOESY experiments, ECD spectra, and biogenic pathway. The subsequent HPLC–MS analysis for the crude extracts of Δ*oxaL* deletant strain by different organic solvents (Supporting Information Fig. S3) indicated that **11** was naturally occurring compound, rather than artificial product. Interestingly, the gene that encodes methyltransferase is absent in the *oxa* cluster. Therefore, compound **11** would likely to be generated by enzyme-catalysed reaction of methyltransferase encoded by gene out of the gene cluster.

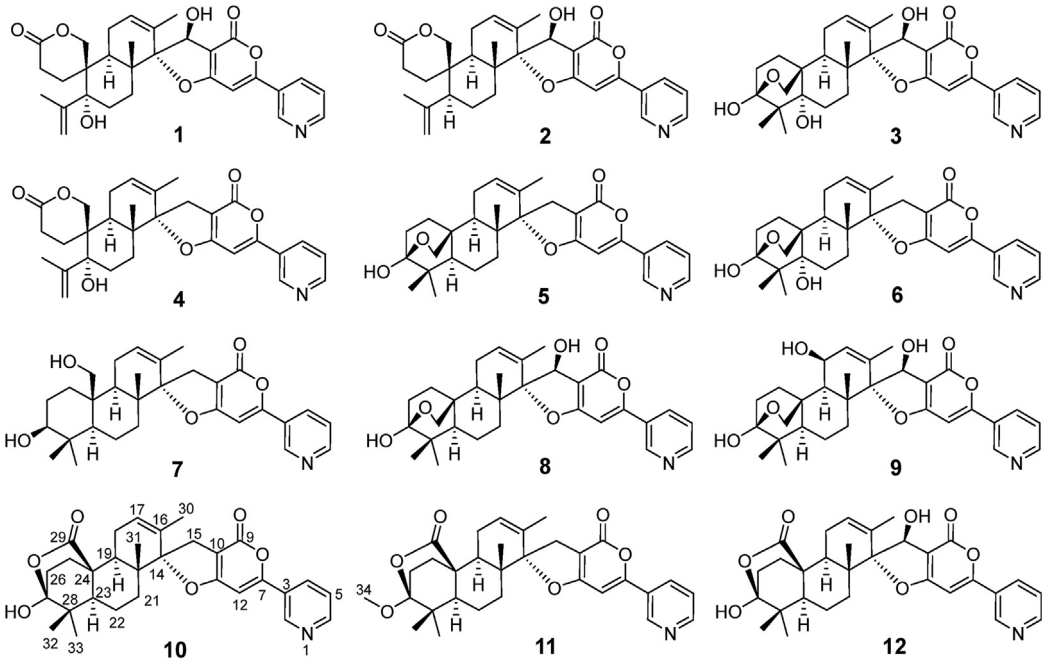

Figure 3 Structures of **1**−**12** isolated from the parental strain, deletants, and *Penicillium* sp. CPCC 400786.

We mapped the steps from **5** to **1** by focusing on the assortment of *oxaK* present in the gene cluster. The chemical investigation of the Δ*oxaK* mutant led to the identification of three known decaturin analogs, decaturin F (**7**)[44], decaturin B (**8**)[37], and 18-hydroxydecaturin B (**9**)[41], and one new decaturin derivative, decaturin J (**12**). Structurally, all isolated compounds lack the C-23 hydroxyl group, consistent with the bioinformatic prediction of OxaK participating in C-23 hydroxylation.

Compound **12** exhibited the HRESIMS peak at *m/z* 520.2358 $[M+H]^+$, in accordance with the molecular formula $C_{30}H_{33}NO_7$, implying that an OH group may be introduced compared to **10**. The ^1H and ^{13}C NMR data (Table S4) of **12** were similar to those of **10**. The obvious difference was the presence of an oxygenated methine (δ_H 5.19; δ_C 73.0) in **12** instead of one methylene (δ_H 3.06, 2.89; δ_C 27.8) in **11**, indicating the introduction of an OH group at the C-15 position, which was further supported by the HMBC correlations from H-15 to C-9, C-10, C-11, C-14, C-16, and C-20. The stereochemistry of **12** was proposed to be the same as **10** and **11** due to the similar NMR values (Table S4) and consideration of the biogenetic origin.

2.3. *Identification of OxaL as hydroxylase in the biosynthesis of oxalicine B (**1**)*

We characterized the C-15 hydroxylation step catalyzed by cytochrome P450 OxaL in detail by cloning intronless *oxaL* into a yeast 2 μm expression plasmid for microsomal formation. OxaL was equipped with the optimal redox partner by cloning *oxaL* from *P. oxalicum* cDNA and heterologously expressing it in *Saccharomyces cerevisiae* strain RC01 (*S.c.* RC01), which contains an integrated copy of cytochrome P450 reductase (*At*CPR) from *Aspergillus terreus*[45]. Upon supplementing compound **5** into the yeast *S.c.* RC01 culture expressing *oxaL*, complete conversion into **8** was observed, which was characterized by the same retention time, UV absorption spectrum (λ_{max} 205, 235, and 335 nm), and MS spectrum (*m/z* 504.2386 $[M-H]^-$) (Fig. 4A, traces ii and iii, Fig. 4B, ii). Microsomal fractions comprising the overexpressed OxaL were purified from a 3-day culture of the yeast mutant. In the *in vitro* biochemical experiment in which 0.5 mmol/L **5** and 2 mmol/L NADPH were supplemented with yeast microsomes (20 mg/mL total protein concentration), conversion of **5** to **8** was detected using UPLC−MS (Fig. 4C, trace ii). These results provide evidence for the role of OxaL in the oxidative insertion of **5** to produce **8**. Furthermore, compounds **4**, **6**, and **7** were then incubated with the *S.c.* RC01 strain transformed with *oxaL*; however, only compounds **4** and **6** resulted in the limited conversion of **1** (*m/z* 564.2224 $[M+HCOOH-H]^-$) and **3** (*m/z* 566.2399 $[M+HCOOH-H]^-$ and *m/z* 520.2348 $[M-H]^-$) based on UPLC−MS analysis, including feed experiments and *in vitro* biochemical assays with purified microsomes of the *S.c.* RC01 mutant strain (Fig. 4B, traces i and iii, Fig. 4C, traces i and iii). However, compound **7** was not converted into any further oxidized metabolites. During the biosynthetic pathway of 15-deoxyoxalicine B (**4**), compound **7** was confirmed as the key on-pathway intermediate decaturin F, in which OlcF might catalyze **7** to yield the 29-hydroxyl-27-one intermediate and subsequently form decaturin C (**5**)[16], indicating that OxaL might participate in catalysis during oxalicine B (**1**) biosynthesis after the OxaF enzymatic step.

A feasible mechanism of the cytochrome P450 OxaL-catalyzed biotransformation to yield the on-pathway intermediate decaturin B (**8**) is shown in Fig. 4D. The hydrogen atom at C-15 is abstracted by the key ferryl-oxo intermediate ($Fe^{IV}=O$, porphyrin π cation radical) to convert radical molecule **A**. Reactive intermediate **A** undergoes oxygen rebound to produce **8**. The reactions led to the formation of a ferric haem centre and continue the catalytic cycle of OxaL with the collaboration of *At*CPR. The iron-oxo species generated from the subsequent P450 cycle undergo a homolytic displacement of OH that returns the resting enzyme. These results confirmed that OxaL is indeed the enzyme that might accept **5** to perform P450-catalyzed hydroxylation[46−48].

2.4. *In vitro biochemical characterization of the hydroxylase OxaK*

We carried out *in vitro* biochemical assays using heterologously expressed OxaK with *Escherichia coli* Transetta (DE3) as host, and 6 × His-tagged OxaK was purified to homogeneity to obtain further insights into the OxaK-catalyzed reaction (Supporting Information Fig. S4)[24,25,49]. Bioinformatic analyses revealed that OxaK is homologous to members of the phytanoyl-CoA dioxygenase (PhyH) superfamily, which requires Fe(II) and α-ketoglutarate (α-KG) for its catalysis (Fig. 5D)[16,28]. Therefore, OxaK was incubated with individual substrates, including **2**, **5**, **7**, **8**, and **9**, as well as in the presence of $FeSO_4$ and α-KG. The *in vitro* assay indicated that OxaK accepted **8** as a substrate, and HPLC analysis showed the appearance of a new peak. A detailed comparison of the retention time, UV absorption spectrum and MS peaks (*m/z* 566.2389 $[M+HCOOH-H]^-$) therefore confirmed that the new peak was 15-hydroxydecaturin A (**3**), which is a biosynthetic intermediate isolated from the Δ*oxaB* deletant strain (Fig. 5A, trace iv). In addition, 18-hydroxydecaturin B (**9**) was completely converted into oxidized product **13** featuring a hydroxyl moiety at C-23 (*m/z* 582.2331 $[M+HCOOH-H]^-$), consistent with our prediction (Fig. 5A, trace v, Fig. 5B). The enzymatic reactions could proceed in the absence of exogenous Fe(II), perhaps due to the residual ferrous ion bound to OxaK, and were completely abrogated in the absence of cofactor α-KG, confirming its metal and α-KG dependencies (Supporting Information Fig. S6)[25]. These results supported the proposal that OxaK demands Fe(II) and α-KG for enzymatic catalysis and can accept **8** and **9** as substrates to catalyze oxidation reactions.

Next, we conducted an *in vitro* biochemical reaction using molecules **2**, **5**, and **7** to further understand the catalysis by the hydroxylase OxaK. Interestingly, when decaturin F (**7**) was incubated with OxaK, new product **14** with a molecular weight 16 amu larger than that of **7** was obtained, suggesting that **14** is an oxidized product of **7** (Fig. 5A, trace iii, Fig. 5C, iii). When recombinant OxaK and **5** were incubated under the same conditions described above, the C-23 hydroxylated product decaturin A (**6**) was obtained with low efficiency (Fig. 5A, trace ii, Fig. 5C, ii). Additionally, oxalicine A (**2**) obtained from strain *Penicillium* sp. CPCC 400786 by our team was also used to test the OxaK-catalyzed reaction[50]. Coincubation of **2** with OxaK as well as the necessary cofactors (α-KG and Fe^{2+}) led to the formation of a low amount of the expected product, oxalicine B (**1**) (Fig. 5A, trace i, Fig. 5C, i), suggesting that stereospecific spiro-forming oxalicine A (**2**) is not easily oxygenated at C-23 by OxaK.

As observed in other Fe(II)/α-KG-dependent dioxygenases, OxaK shares a conserved 2-His-1-carboxylate iron-binding facial triad (H_{103}, D_{105}, H_{270}) (Supporting Information Fig. S5)[20,25,34], and consequently, the iron atom at this site might function in OxaK-catalyzed oxygenation. The proposed mechanism for hydroxylation is described below (Fig. 5E). First, α-KG and molecular oxygen are integrated to the active triad site of the oxygenase, and the subsequent oxidation of Fe(II) and α-KG could generate the highly reactive Fe(IV)-oxo intermediate and succinate with a release of free CO_2. Next, the hydrogen atom is

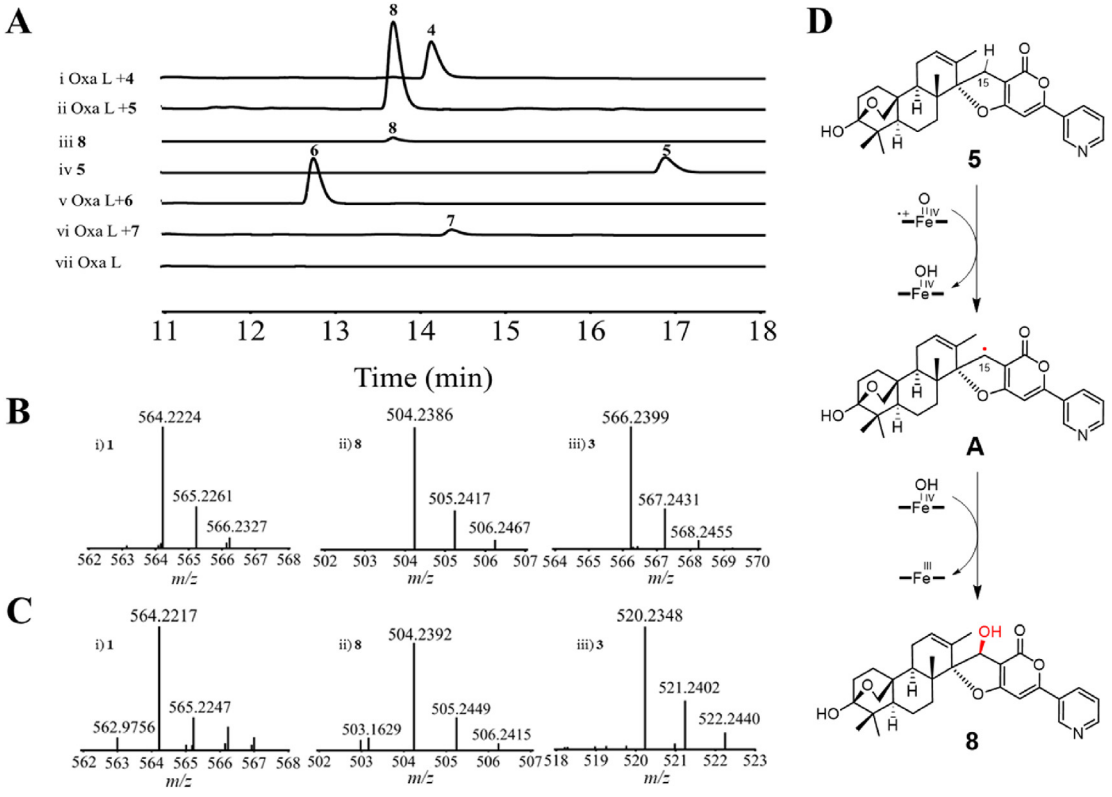

Figure 4 Biochemical assay and proposed mechanism of cytochrome P450 OxaL. (A) HPLC traces of the OxaL-catalyzed feed experiment. (B) UPLC−MS data for products of the OxaL-catalyzed feed experiment. (C) UPLC−MS analysis of the products during the *in vitro* biochemical assays of yeast microsomes in the presence of **4**−**6**. (D) Proposed reaction mechanism of cytochrome P450 OxaL. The chromatograms were monitored at 310 nm.

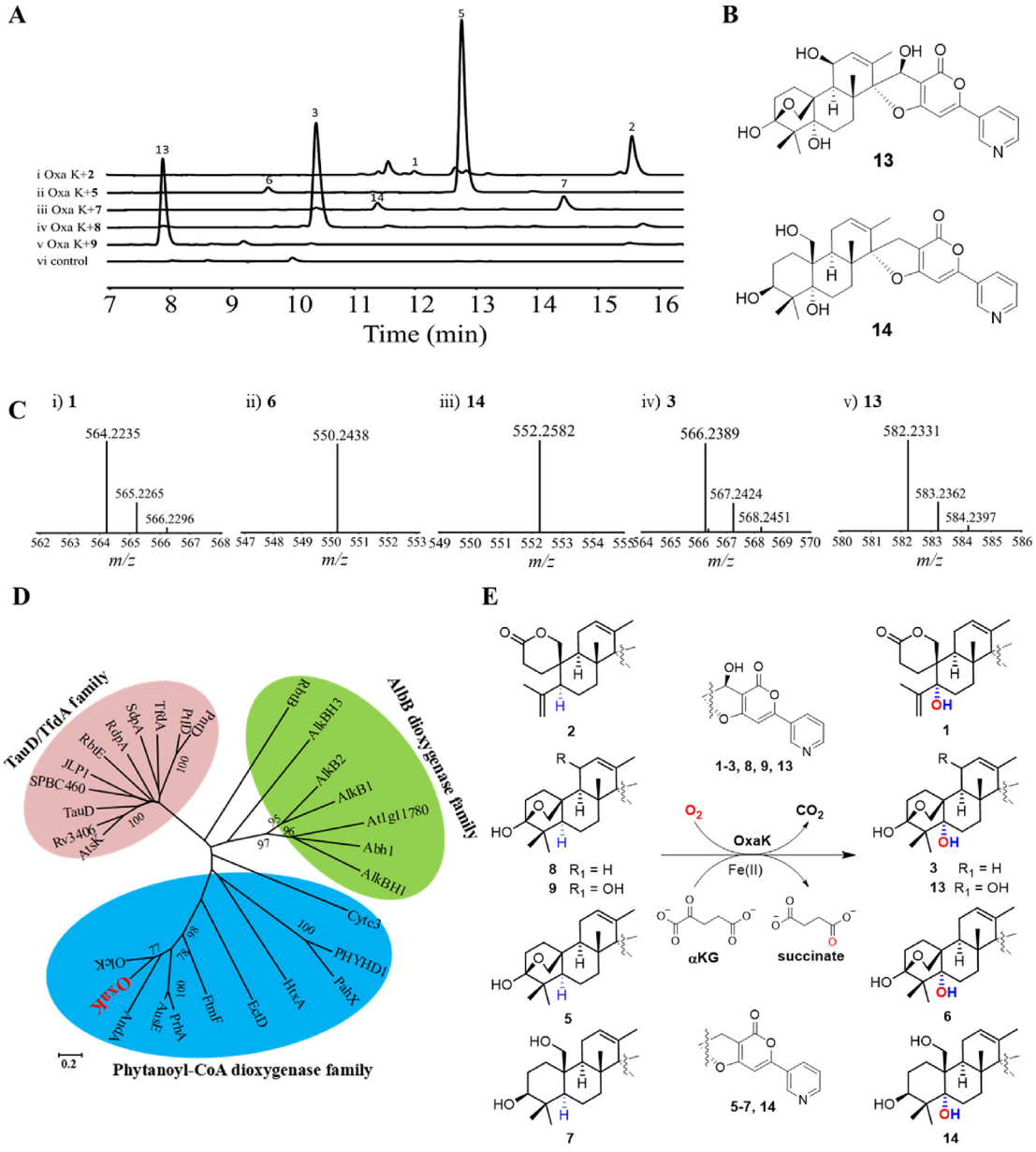

Figure 5 *In vitro* biochemical assay and phylogenetic analyses of hydroxylase OxaK. (A) HPLC traces of the OxaK-catalyzed reactions. (B) Structures of the two new OxaK enzymatic products. (C) UPLC−MS analysis of the products of the OxaK-catalyzed reactions. (D) Phylogenetic analyses of OxaK with Fe(II)/α-KG-dependent dioxygenases. (E) Proposed reaction mechanism and substrate scope of hydroxylase OxaK. The chromatograms were monitored at 310 nm.

abstracted from C-23 and hydroxylated at C-23 to form hydroxylated products. Collectively, these studies confirmed the function of OxaK as an archetype hydroxylase and revealed that the enzyme might finalize the installation of the hydroxyl group during oxalicine B (**1**) biosynthesis with a remarkable substrate scope, including on-pathway intermediates (or related compounds) and off-pathway intermediates (Fig. 5E).

2.5. *Verification of OxaB and identification of 15-hydroxdecaturin A as a biosynthetic intermediate*

Next, we performed biochemical characterization using the same method as for the OxaL system to further investigate the role of the cytochrome P450 OxaB. *At*CPR was reported previously to participate in the coupled reduction of fungal cytochrome P450s in yeast for biotransformation[51,52]. The enzymatic activity of OxaB was observed by supplementing 1 mg of substrate **3** into 20 mL of *S. cerevisiae* culture expressing OxaB and *At*CPR. Although bioconversion exhibited low efficiency, a slight conversion of **3** to **1** (*m/z* 564.2206 [M+HCOOH−H]$^-$) was characterized using the UPLC−MS platform when **3** was fed to the culture (Fig. 6B, trace i), while no biotransformation was detected in the control RC01 yeast culture expressing only *At*CPR. In an *in vitro* biochemical assay in which 0.5 mmol/L **3** and 2 mmol/L NADPH were incubated with OxaB microsomes (20 mg/mL total protein concentration), HPLC analysis showed the limited conversion of **3** to **1** with low efficiency (Fig. 6A, trace iii), further retention time and UV absorption spectrum comparison characterized the formation

of final product **1** from intermediate **3** by microsomal OxaB (Fig. 6A, trace iii). Additionally, oxalicine B (**1**) was detected using UPLC−MS (Fig. 6B, ii). The comparatively lower transformation rate and requirement of OxaB microsomes for conversion might be due to the low expression of OxaB in *S. cerevisiae*[52]. Moreover, we also fed 1 mg of substrates **5**, **6**, and **8** to 20 mL of yeast culture expressing *At*CPR and OxaB, respectively, and the conversion of **5** to 15-deoxyoxalicine A, **6** to **4**, and **8** to **2** was observed using UPLC−MS (Fig. 6B, iii, iv, v, Fig. 6C).

Successful biotransformation of **3** to **1** confirmed that OxaB is the sole oxygenase that could convert **3** to the formation of spirolactone framework **1**. The oxidative rearrangement might be initiated by C-32 or C-33 hydroxylation *via* the typical hydrogen abstraction/oxygen rebound mechanism to form C-32 or C-33 hydroxylated intermediate **A**. The latter reaction occurs *via* intermediate **A** and promotes the subsequent ring-opening rearrangement through C_{27}−C_{28} bond rupture and dehydration to generate **1** (Fig. 6D, Route A)[16]. A similar mechanism is proposed for the cytochrome P450 LovA in the lovastatin pathway, whereby allylic alcohols initially emerge and then dehydrate to yield monacolin L[53]. An alternative mechanism is that OxaB might initiate the oxidative rearrangement cascade *via* dehydrogenation, and the hydrogen atom at C-32 or C-33 is abstracted by the key ferryl-oxo intermediate (Fe^{IV}=O, porphyrin π cation radical) to form radical species **B** (Fig. 6D, Route B)[46−48]. The subsequent radical rearrangement results in the cleavage of the C−C bond at C-27/C-28 and the formation of double bonds (C_{28}=C_{32} or C_{28}=C_{33}) and carbon radical at C-27 (intermediate **C**). This redical **C** is then converted into a germinal diol (intermediate **D**) by rebinding of the hydroxyl radical, followed by dehydration reaction to produce the spiro unit of **1**. A similar mechanism has been proposed for the P450-catalyzed reaction process, *e.g.*, *Catharanthus roseus* P450 72A1-catalyzed C−C bond cleavage in the conversion of loganin to secologanin[54,55], VrtK-catalyzed spirocyclization of the geranyl moiety during biosynthesis from previridicatumtoxin to viridicatumtoxin[56].

2.6. *The late-stage cascade of oxidative modifications generates complexity that affords* ***1***

Based on the chemical structures of the isolated compounds, new metabolites (**10**−**12**) were obviously excluded from the analysis determining on-pathway intermediates (Fig. 3). We then added **2**−**9** to the Δ*oxaA*-OE:*olcL* mutant strain to confirm whether these isolated molecules are on pathway intermediates (Supporting Information Fig. S7), yet feeding **2**−**8**, but not **9**, restored the biosynthesis of **1**. Therefore, compounds **2**−**8** were determined to be in the pathway, and **9** represents a shunt product. Further *in vitro* biochemical assays of the three characterized oxidative enzymes in this work revealed a late-stage cascade of oxidative modifications for oxalicine B (**1**), as shown in Fig. 7. The pathway starts with the conversion of decaturin F (**7**) to decaturin C (**5**) by the SDR enzyme OxaF[16]. The beginning oxidation of **5** by cytochrome P450 monooxygenase OxaL includes C−H hydroxylation at the C-15 position in the furan ring to yield **8**. Subsequently, an additional oxygenation reaction catalyzed by the α-KG dioxygenase OxaK installs the C-23 hydroxyl group in **3**. On-pathway intermediate **3** is then subjected to successive oxidative cleavage/rearrangement occurring *via* either hydroxylation or radical abstraction mechanisms. This reaction is catalyzed by the P450 monooxygenase OxaB and then furnishes the characteristic spirolactone core skeleton to yield **1** (Fig. 7A)[16].

The Δ*oxaB* deletant strain accumulated 15-hydroxdecaturin A (**3**), which possesses two additional hydroxyl groups compared with **5**. The data imply that both OxaK and OxaL are involved in the biotransformation of **5** to **3**. Deletion of the C-23 hydroxylation-catalyzed oxygenase coding gene *oxaK* resulted in the accumulation of **7**−**9**. Interestingly, an *in vitro* biochemical assay further confirmed the hypothesis that **8** structurally resembles the native substrate of OxaK, which incorporates a hydroxyl group at C-15 of **5**, suggesting that OxaL participates in the conversion of **5** to **8**. Notably, compound **9** is a C18-hydroxylated version of **8**, which further manifests as an OxaK enzymatic reaction following the OxaL-catalyzed step (Fig. 3). Furthermore, the metabolomic profile of the Δ*oxaL* mutant strain exhibited the accumulation of **4**, **5**, and **6**, and OxaL was also proven to catalyze **4** and **6** based on an *in vitro* biochemical assay with *S.c.* RC01-*oxa*L microsomes or feeding experiments (Fig. 4B and C). In contrast, we validated that OxaL is extremely specific for C-23 unoxygenated intermediate **5** based on a feeding experiment of *S.c.* RC01 culture expressing *oxaL* (Fig. 4A, trace ii). Hence, we proposed that OxaK-catalyzed hydroxylation occurs after the incorporation of the hydroxyl group at C-15 in **5**, followed by oxidative rearrangement dominated by the downstream oxygenase OxaB, which should be the mainstream biosynthetic pathway *in vivo*.

Notably, the on-pathway intermediate oxalicine A (**2**) was transformed into **1** by the oxygenase OxaK, although at low efficiencies (Fig. 5A, trace i); however, another possibility of a late-stage biosynthetic pathway of **1** was suggested (Fig. 7B). Yaegashi and coworkers reported that 15-deoxyoxalicine A was recovered when decaturin C (**5**) was fed to the Δ*olcK* or Δ*olcL* deletant, implying that the previously reported hydroxylase OlcK might be involved before the OlcB (OxaB homolog) step during 15-deoxyoxalicine B (**4**) biosynthesis[16]. As described above, the most advanced intermediate **5** was converted to intermediate **6** at a low level by the oxygenase OxaK (Fig. 5A, trace ii). Intriguingly, a similar finding was observed for the cytochrome P450 OxaL, which accepted **4** or **6** as a substrate awaiting further hydroxylation but not the native substrate. Feeding Δ*oxaA*-OE:*olcL* experiments indicated that **2**−**4**, **6**, and **8** supplementation restored the biosynthesis of **1**, thereby suggesting that these compounds are also intermediates *in vivo*. Taken together, three possible shunt pathways from intermediate **5** to **1** might occur *in vivo* or during biochemical transformation *in vitro*, as shown in Fig. 7B.

2.7. *Bioactivities evaluation*

All isolated compounds were assessed for anti-IAV bioactivities. Compounds **3**−**12** exhibited potent anti-IAV (H1N1) activities with corresponding IC_{50} values in the range of 4.0−19.9 μmol/L (Table 1), which were superior to the positive control ribavirin (IC_{50} = 28.2 μmol/L). In particular, compounds **4**, **6**, and **12** were approximately 6 times stronger than ribavirin.

3. Discussion

In this report, we characterized three oxygenases in the late-stage biosynthetic pathway that transform multicyclic hemiketal decaturin C (**5**) into richly decorated oxalicine B (**1**). The highly oxidized α-pyrone portion of **1**, which is also present in the molecule arisugacins derived from *Penicillium* sp. FO-4259, has been the subject of increasing synthetic efforts[35,38,57]. Nevertheless, the regioselective oxygenation of bispirocyclic (C-14 and C-

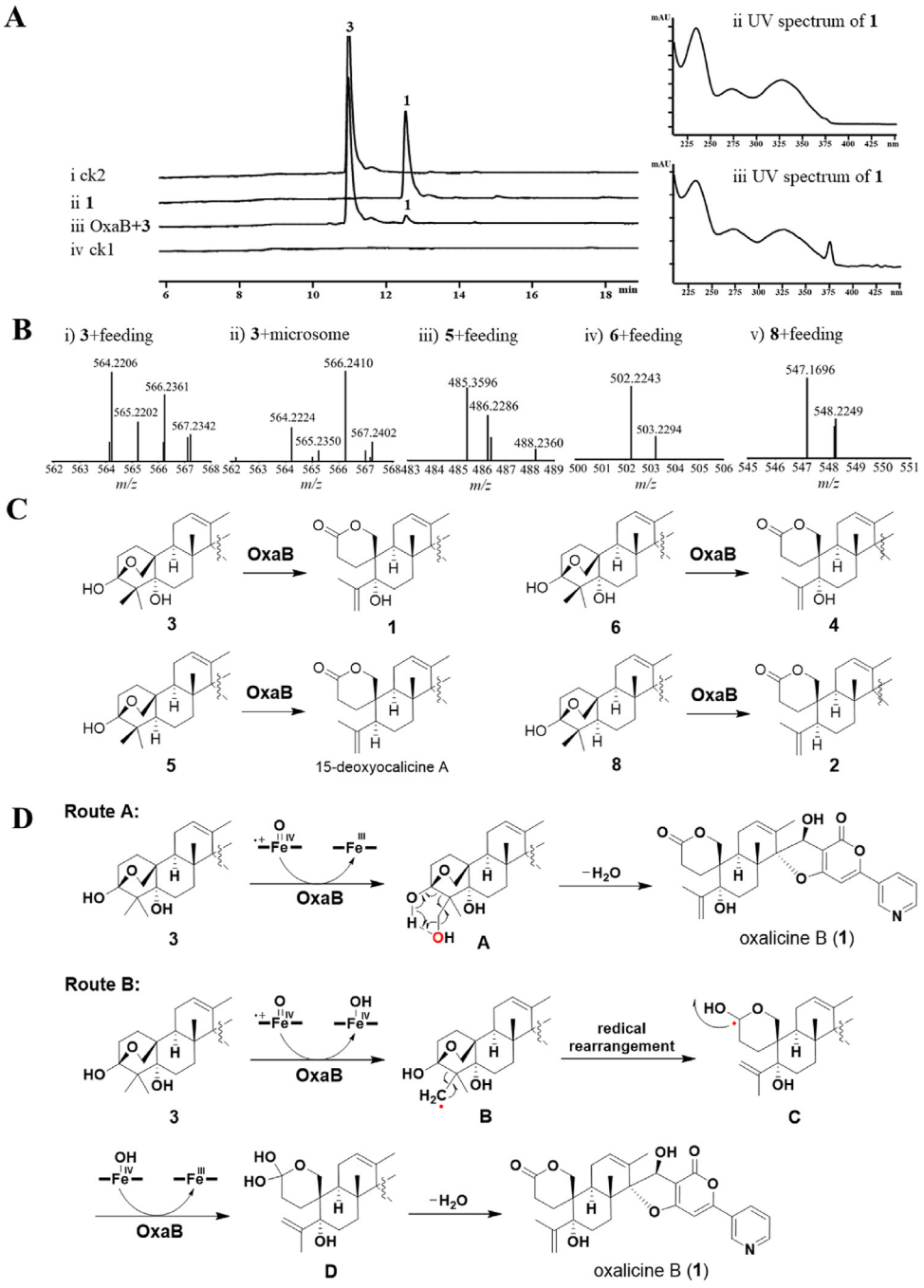

Figure 6 Biochemical assay and proposed mechanism of cytochrome P450 OxaB. (A) HPLC trace of the *in vitro* biochemical assay of microsomal OxaB, UV spectrum comparison of **1** and forming product. (B) UPLC−MS analysis of the products of the OxaB-catalyzed feeding experiment and *in vitro* biochemical assays of yeast microsomes expressing OxaB and *At*CPR. (C) The substrate and products of P450 monooxygenase OxaB. (D) Proposed reaction mechanism of cytochrome P450 OxaB. The chromatograms were monitored at 310 nm.

24) scaffolds in **1** is challenging. Most impressively, OxaL alone catalyzes the installation of the C-15 hydroxyl group in **5** to afford intermediate **8** (Fig. 7), and thus the present study is the first to provide a biochemical and genetic evidence for the biosynthesis of oxalicine derivatives with 15-OH groups[1]. The hydroxylation reaction catalyzed by OxaK must also function in the transformation of **8** into **3**, which is structurally similar to **8**, except for the supplementary hydroxyl moiety at C-23 (Fig. 7). OxaB was determined to be the key oxygenase in the construction of the spiro-fused cyclic framework in **1**. In the present study, several on-pathway intermediates, including two oxalicine analogs (**2** and **4**) and five decaturin analogs (**3**, **5**−**8**), were characterized, while shunt products/off-pathway intermediates (**9**−**12**), including three new intermediates (**10**−**12**), were ruled out. Subsequent feed experiments and genetic and biochemical identifications allowed us to propose late-stage oxidative steps for **1** (Fig. 7A). We also examined variations in this pathway, and the different intermediates were involved in each of the other three pathways, as

shown in Fig. 7B. We believe that all four pathways are accessible and that path A is essential. These pathways deduced from our investigations have broadened our understanding of the biosynthesis of oxalicines[1,16,35].

Oxidative morphing of terpenoid scaffolds is common in meroterpenoids[27,34]. Fe(II)/α-KG-dependent dioxygenases and cytochrome P450 enzymes are commonly dispersed in the metabolic pathways of NPs and have been demonstrated to catalyze unusual reactions, including reported examples of functional group rearrangement/migration and heterocycle formation[1,27,58]. Dozens of oxygenases have been stated to catalyze multistep oxidation at diverse carbon atoms of chemical molecules, bringing about drastic structural transformations[11,17,20,24,25,33,52]. The presence of chemistry in nature is well represented by the structures of oxalicines, which possess a distinct pyridinyl-α-pyrone polyketide fused to a diterpenoid substituent, multiple stereogenic centers, and particularly a characteristic bispiranic ring framework[16]. Nevertheless, no report has described the total synthesis of oxalicines[35]. Regarding the biosynthesis of 15-deoxyoxalicine B in *P. canescens*, Yaegashi and coworkers envisaged a direct link between the compound and biosynthetic gene cluster *olc*[16]. However, biochemical evidence for the characterization of key oxygenases, including cytochrome P450 OlcB and hydroxylase OlcK, is unavailable[16]. In the present study, *in vitro* biochemical assays of OxaB and OxaK were performed and confirmed their functions as cytochrome P450s and hydroxylases, respectively. In addition, the incorporation of the hydroxyl group into C-15 with the appropriate enantiomer makes the late-stage biosynthesis of the oxalicine B (**1**) complicated, which also highlights the desirability of exploring the potential of other members of α-pyrone meroterpenoids, such as breviones[35,59]. Based on our studies, we propose that cytochrome P450 OxaL functions as a hydroxylase, which solves the mystery of C-15 hydroxylation during oxalicine B biosynthesis. Furthermore, the multifunctional cytochrome P450 OxaB is the sole enzyme involved in the consecutive series of chemically featured catalytic processes. The P450 oxygenase might follow two catalytic mechanisms: one is that it starts the oxidative transformation of **3** involving C-32 or C-33 hydroxylation, followed by oxidative ring-opening accompanied to elimination of a water molecule and oxidative rearrangement (Fig. 6C, Route A)[16]. However, the absence of a C-32 or C-33 hydroxylated intermediate in the biochemical assay implies that **3** might preferentially abstracts the hydrogen atom at C-32 or C-33 to form carbon redical **B**, and redical **B** undergo redical rearrangement to achieve the C−C double bond formation (C-28/C-32 or C-28/C-33) and C−C bond cleavage (C-27/C-28), followed by hydroxylation and dehydration to generate product **1** (Fig. 6C, Route B). Thus, hemiketal intermediate **3** is converted into **1** with the aid of OxaB, which would provide insights into the chemical synthesis of these fascinating oxalicines. Additionally, the conversions of **5** to 15-deoxyoxalicine A, **6** to **4**, and **8** to **2** by OxaB suggest that the oxygenase might accept different substrates, regardless of whether 15-OH or 23-OH groups are present.

To our knowledge, this report is the first to document the biochemical characterization of OxaK and its role during the biosynthesis of oxalicines. We examined substrate variations of OxaK, including a prehemiketal intermediate (**7**), hemiketal intermediates (**5** and **8**), and posthemiketal intermediate (**2**). Interestingly, oxygenase might recognize various substrates of three different phases (Fig. 5A and E). Derived from our experimental data, we presume that the mechanism proposed by Yaegashi and coworkers should be revised to a mechanism in which one enzyme, OxaK, mediates hydroxylation instead of two enzymes [a 2-oxoglutarate-Fe(II) oxygenase, OlcK, and a putative MFS (major facilitator superfamily) transporter] coupled to the generation of hydroxyl groups at C-23[16]. In the course of our studies, we identified that the mutant Δ*oxaA*:OE:*olcL* derived from Δ*oxaA* deletant was a better choice than the Δ*oxaA* mutant for feed experiments, in which the putative MFS transporter coding gene *olcL* from the gene cluster *olc* for biosynthesis of 15-deoxyoxalicine B (**4**) was overexpressed[16]. Additionally, this result suggested that OlcL might function as an MFS transporter only. Further investigation and downstream application of the MFS transporter OlcL for metabolic mining or increasing the

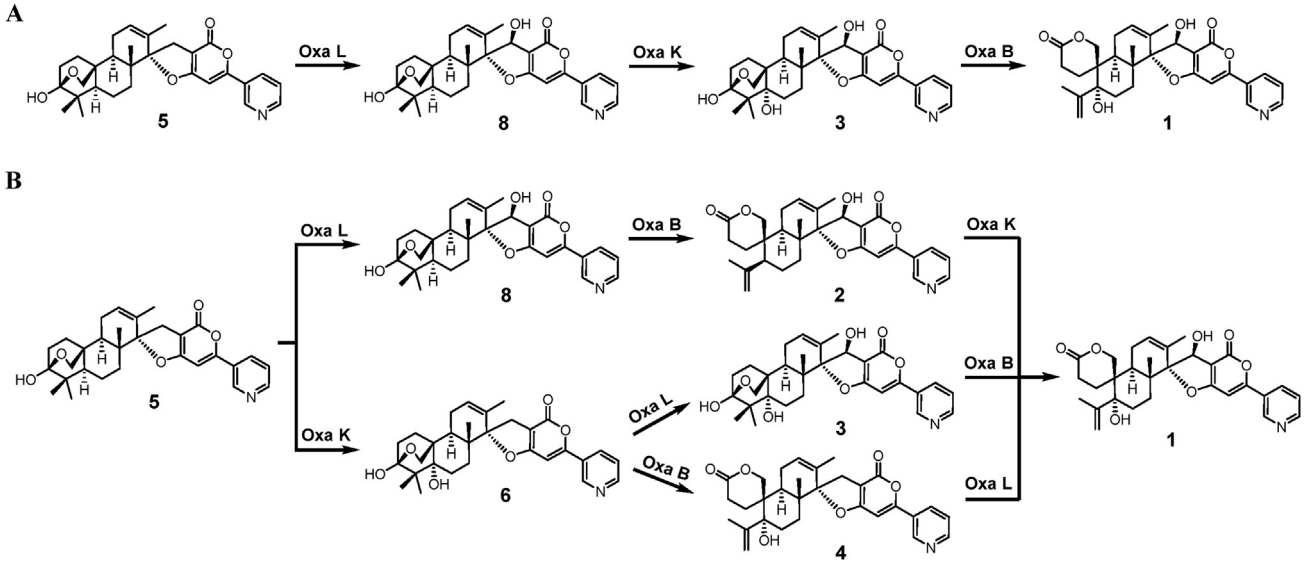

Figure 7 The proposed late-stage biosynthetic pathway of oxalicine B. (**1**) based on biochemical and genetic evidence. (A) The main biosynthetic pathway *in vivo* from intermediate decaturin C (**5**) to **1**. (B) Three possible shunt pathways from intermediate **5** to **1** that might occur *in vivo* or biochemical transformation *in vitro*. OxaL, cytochrome P450; OxaK, α-KG dioxygenase; OxaB, cytochrome P450.

Table 1 The anti-IAV activities of **3**−**12**.

Compd.	IC_{50} (μmol/L)	CC_{50} (μmol/L)
3	7.43 ± 2.50	>100
4	4.03 ± 1.11	>100
5	6.61 ± 1.91	>100
6	4.56 ± 1.06	>100
7	18.37 ± 5.16	>100
8	9.08 ± 0.27	>100
9	19.90 ± 4.53	>100
10	7.48 ± 1.40	>100
11	7.24 ± 1.95	50.51 ± 2.26
12	4.48 ± 0.68	>100
Ribavirin	28.21 ± 4.36	>100

production of oxalicines in *P. oxalicum* is warranted and has already been performed in our lab.

4. Conclusions

Overall, we have elucidated the roles of three oxygenases, OxaL, OxaK, and OxaB, involved in the biosynthesis of oxalicine B (**1**). Among the three oxygenases, the cytochrome P450 OxaL catalyzes the installation of a hydroxyl group at C-15. We also characterized the function of OxaK as a hydroxylase that results in the conversion of C-23 hydroxylation. The catalytic substrate promiscuity of OxaK therefore augments the already impressive chemical versatility of this fascinating category of enzymes. Fascinatingly, the hemiketal intermediates during the biosynthesis of oxalicine B (**1**) undergo further multistep oxidative rearrangement catalyzed by the cytochrome P450 OxaB, and OxaB potentially accepts various substrates and exhibits a broad substrate scope. In addition, compounds **3**−**12** exhibited potent anti-IAV activities, which indicated the potential of these molecules acting as promising anti-IAV lead compounds. This report has uncovered tailoring modifications in the late-stage biosynthetic pathway of **1** and will provide opportunities for the derivatization of oxalicines and decaturins using enzymatic strategies.

5. Experimental

5.1. Strains and cultivation

The *P. oxalicum* strain and the derived mutants utilized in the study are shown in Supporting Information Table S3 and are deposited in the China Pharmaceutical Culture Collection Center. All the wild-type and mutants were cultured on potato dextrose agar (PDA, BD) at 28 °C. For gene knockout of *P. oxalicum*, PDA (BD) with 1.2 mol/L sorbitol and 250 μg/mL hydromycin was used for protoplast regeneration and antibiotic selection. For *olcL* gene overexpression, 600 μg/mL G418 was employed for antibiotic resistance selection. *E. coli* Trans1-T1 (TransGen) was applied for standard molecular cloning, and Transetta (DE3) was utilized for enzyme expression. *S. cerevisiae* BJ5464-NpgA was used for *in vivo* yeast DNA recombination cloning[45]. *S. cerevisiae* strain RC01 was used as a heterologous expression host, which contains a chromosome-integrated gene encoding a cytochrome P450 reductase (CPR) from *Aspergillus terreus*[47]. YPD (BD) was applied for the regular cultivation of yeast and mutants at 30 °C. SD dropout medium was utilized for the selection of yeast mutant strains.

5.2. AntiSMASH and bioinformatic analysis

Genome mining and detection of natural product biosynthetic gene clusters in *P. oxalicum* was performed with the antiSMASH 6.0 platform[49]. The softberry FGENESH program was used for predictions of the coding sequences[58]. The function of the coding sequence was predicted by comparsion with homologous proteins in the NCBI database. The functional assignment of the protein was further analyzed using the Phyre2 database.

5.3. General approach for molecular manipulation

P. oxalicum genomic DNA was extracted using CTAB buffer as performed elsewhere[60]. Polymerase chain reactions were performed using Q5 DNA Polymerase (NEB) or Phanta® Max Super-Fidelity DNA polymerase (Vazyme). Restriction endonucleases were used following the recommended protocol by the manufacturer (New England Biolabs). RNA extraction was performed using a PureLink™ RNA Mini Kit (Invitrogen), and the Easy-Script® Reverse Transcription System for RT-PCR (Transgen) was applied to synthesize complementary DNA (cDNA) as described by the manufacturer. PCR products were subcloned into a pEASY®-Blunt Vector (Transgen) and verified by sequencing. Gene primers were synthesized by Sangon Biotech (Shanghai) Co., Ltd. and are shown in Supporting Information Table S3. *In vivo* recombination cloning was applied by transforming the yeast with PCR fragments and a linearized 2 μm plasmid vector using an *S.c*. Frozen-EZ Yeast Transformation II Kit (ZYMO).

5.4. Chemicals and chemical analysis

All solvents and chemicals used in this study were of analytical grade (for extraction) or LMS grade (for LC−MS analysis). For the production of **1** and other metabolites, *P. oxalicum* and mutant strains were cultivated on MEPA medium (malt extract broth, BD; 0.3% soy flour, agar 15 g/L). Total RNA for RT-PCR was extracted from *P. oxalicum* grown on MEPA after 5 days of cultivation. For chemical complementation of the Δ*oxaA*-OE:*olcL* mutant, purified compounds were added to the MEPA medium at 0.2 mg/mL individually. HPLC analysis was performed on an Agilent 1290 (YMC-C_{18} column, 5 μm, 4.6 mm × 250 mm) and separated on a 5%−95% (*v*/*v*) acetonitrile-H_2O linear gradient in H_2O containing 0.05% formic acid (*v*/*v*) at a flow rate of 1 mL/min. All LC−MS analyses were performed on a Waters ACQUITY UPLC-Class-MS with a Xevo-G2-S Q-TOF mass detector (Waters ACQUITY UPLC-BEH-C_{18}, 1.7 μm, 2.1 mm × 100 mm) using positive and negative mode electrospray ionization with a linear gradient of 10%−20% acetonitrile/H_2O (*v*/*v*, 0.02% formic acid) in 5 min followed by 20% acetonitrile/H_2O (*v*/*v*, 0.02% formic acid) for 2 min and 20%−100% acetonitrile/H_2O (*v*/*v*, 0.02% formic acid) for 18 min with a flow rate of 0.5 mL/min ^{1}H NMR, ^{13}C NMR and 2D NMR spectra were obtained on a Bruker AVIII-600 spectrometer at the Institute of Materia Medica, Chinese Academy of Medical Sciences & Peking Union Medical College.

5.5. Construction of P. oxalicum mutants

All the deletants of the *P. oxalicum* strain were obtained by the hygromycin split-marker homologous recombination strategy[45]. Transformation of strain 114-2 was carried out by the standard protoplast-polyethylene glycol (PEG) strategy previously

reported[49]. Transformants were transformed into a selective PDA medium to confirm the genotype by PCR characterization. The primers used for the construction of deletion cassettes and diagnostic PCRs are listed in Table S1. The comparison of amplicon size between the gene replaced by the resistance gene and the target gene enabled us to characterize the correct gene deletants. All deletants were constructed by substituting individual targeted gene sequences with the hygromycin selective marker in the parental strain (wild type) of *P. oxalicum*. The *Agrobacterium tumefaciens*-mediated transformation of *P. oxalicum* was performed as reported previously with minor modifications[58]. The *A. tumefaciens* AGL-1 strain was transformed with the OE:*olcL* overexpression cassette pZT09 by electroporation. The coculture experiments were performed at 28 °C for 72 h. The randomly selected mutants were then transferred to selection PDA plates containing G418 (600 μg/mL) and cefotaxime (200 μg/mL) as selective antibiotics. The primers used for constructing the gene overexpression cassette and diagnostic PCR are listed in Table S1.

5.6. Heterologous expression and purification of OxaK

The *oxaK* transcript was obtained by RT-PCR and verified by sequencing. The DNA fragment of *oxaK* from cDNA was ligated into pET30 (Novagen) digested by *Nde*I and *Hind*III to obtain pZT10. The primers used for PCR amplification are shown in Table S1. Recombinant enzymes were heterologously expressed in *E. coli* Transetta (DE3) and purified by nickel affinity chromatography. The *E. coli* strains were cultivated at 37 °C and 200 rpm in 1000 mL of LB broth supplemented with 50 μg/mL kanamycin. Isopropylthio-*β*-D-galactoside (IPTG, 0.5 mmol/L) was added to induce OxaK expression at an OD_{600} from 0.4 to 0.6 and the culture was further incubated overnight at 20 °C. The culture was then collected by centrifugation (5000 rpm, 10 min), resuspended in 50 mL of lysis buffer (50 mmol/L Tris-HCl, pH 7.5, 0.1 mol/L NaCl, 10 mmol/L imidazole), and subsequently disrupted in a high-pressure homogenizer (ATS Engineering Ltd.) at 1000 bar. Cell debris was removed by centrifugation (13,000 rpm, 30 min, 4 °C). The expressed OxaK was purified by using a High Affinity Ni-Charged Resin FF Prepacked Column (GenScript) in accordance with the manufacturer's protocol. Purified OxaK was concentrated and exchanged into buffer A (50 mmol/L Tris-HCl, pH 7.5, 2 mmol/L DTT) + 20% glycerol with the centriprep filters (Amicon® Ultra) and preserved at −80 °C for biochemical assays. The purified OxaK was detected by SDS-PAGE. The protein concentration was determined with the Bradford assay according to the manufacturer's instructions.

5.7. Assay for OxaK activity

For the *in vitro* enzymatic assay for OxaK activity on compounds **2**, **5**, **7**, **8**, and **9**, the reactions of OxaK were conducted in a 100 μL reaction mixture containing 50 mmol/L Tri-HCl (pH 7.5), 1 mmol/L sodium ascorbate, 1 mmol/L *α*-ketoglutarate, 1.0 mmol/L $(NH_4)_2Fe(SO_4)_2$, 10 μmol/L OxaK, and a 20 μmol/L substrate. The requirement for Fe^{2+} in the reaction was demonstrated by omitting Fe^{2+} in the reaction. After incubation at 30 °C for 12 h, the reactions were extracted twice using 200 μL ethyl acetate, dried and dissolved in 50 μL acetonitrile and subjected to LC−MS analysis as described in Chemicals and Chemical Analysis[49].

5.8. Biotransformation in S. cerevisiae

For biotransformation in *S. cerevisiae* (*S.c.*) expressing OxaB, *S. cerevisiae* strain RC01 harboring the OxaB plasmid was inoculated into 5 mL of Yeast Synthetic Drop-Out medium without leucine[52]. The cells were cultured for 36 h with shaking at 28 °C. One milliliter of seed culture was transferred into 100 mL of YPD (BD) with shaking at 28 °C for 48 h. The *S.c.* culture was collected by centrifugation (4000 rpm, 10 min), resuspended in 10 mL of YPD medium, **3** (1 mg in 10 μL of DMSO) was added, and the *S.c.* culture was cultivated for another 48 h with shaking at 28 °C. The cultures were extracted with ethyl acetate (1:1) two times, and the organic layers were dried *in vacuo* and redissolved in 100 μL of acetonitrile. A 20 μL aliquot of samples was further evaluated by LC−MS according to the protocol interpreted in the Chemicals and Chemical Analysis section. For biotransformation in OxaL-expressing *S.c.*, the culture was performed using the same approach described above and **4**−**7** (0.1 mg in 10 μL of DMSO) was added to the yeast culture.

5.9. Microsome assay for OxaB and OxaL activities

OxaB and AtCPR-containing microsomes for the *in vitro* assay were prepared and performed according to a protocol reported previously[51,52]. For the *in vitro* microsome biochemical assay, 10 mg/mL (wet weight) microsomal fractions containing OxaB and *At*CPR, 1 mmol/L substrate **3**, 2 mmol/L NADPH, and NADPH regeneration system (IPHASE, Beijing) solution A (10 μL) and B (2 μL), and 50 mmol/L Tri-HCl (pH 7.5), were incubated in a 100 μL reaction. The reaction was incubated at 28 °C for 16 h and extracted two times with 100 μL of ethyl acetate. The organic phase was vacuum-evaporated until dry, and the residues were redissolved in 20 μL of acetonitrile, and subsequently analyzed by LC−MS. The quantity of protein in 20 mg/mL microsomes was regulated to be 180 μg/mL using the Bradford assay against a BSA standard curve. For biotransformation in *S.c.* of OxaL, the assay was performed using the same conditions as above, in which **4**−**7** was added as substrate. The reactions were performed using the same method as described above and subjected for detection using LC−MS as described in the Chemicals and Chemical Analysis section.

5.10. Fermentation and extraction

The mutant strains of *P. oxalicum* 114-2 were cultivated on agar plates, each containing approximately 50 mL medium (2% malt extract broth, 2% agar and 0.2% soybean meal). Each plate was inoculated into 200 μL of the spore suspension, and cultured at 28 °C for 7 days. The fermented material was extracted three times with EtOAc, the organic layer was concentrated to dryness under vacuum, and redissolved in 1 mL MeOH, and the sample (5 μL) was analyzed by high performance liquid chromatography analysis. (Agilent 1290, YMC-C_{18} column, 5 μm, 4.6 mm × 250 mm).

5.11. Isolation and characterization of metabolites 3−12

The fermented material of Δ*oxaB* deletant strain was extracted with EtOAc (3 × 3 L) to give the crude extract (12 g), which was performed to silica gel column chromatography (CC) eluting with dichloromethane−acetone gradient (100:0−0:100, *v*/*v*) to give three fractions (Fr.1−Fr.3) on the base of the HPLC analysis. Fr.3

(410 mg) was subjected to Sephadex LH-20 gel CC eluting with CH_2Cl_2−CH_3OH (1:1, *v*/*v*) to produce six fractions (Fr.3.1−Fr.3.6). Fr.3.5 (78 mg) was isolated and purified by semi-preparative HPLC eluting with CH_3CN−H_2O (30:70) at 6 mL/min to yield **3** (36 mg).

The fermented material of Δ*oxaL* deletant strain was extracted with EtOAc (3 × 5 L) to give the crude extract (12 g), which was performed to silica gel CC eluting with dichloromethane−acetone gradient (100:0−0:100, *v*/*v*) to produce six fractions (Fr.1−Fr.6) based on the HPLC analysis. Fr.3 (117.8 mg) was subjected to Sephadex LH-20 gel CC eluting with CH_2Cl_2−CH_3OH (1:1, *v*/*v*) to give twelve fractions (Fr.3.1−Fr.3.12). Fr.3.5 (20 mg) was purified by semi-preparative HPLC eluting with CH_3CN−H_2O (45:55) at 6 mL/min to produce **4** (8.7 mg). Fr.2 (79 mg) was subjected to Sephadex LH-20 gel CC eluting with CH_2Cl_2−CH_3OH (1:1, *v*/*v*) to yield eleven fractions (Fr.2.1−Fr.2.11). Fr.2.5 (16 mg) was further purified by semi-preparative HPLC eluting with CH_3CN−H_2O (45:55) at 6 mL/min to produce **5** (2.3 mg). Fr.5 (115 mg) was subjected to Sephadex LH-20 gel CC eluting with CH_2Cl_2−CH_3OH (1:1, *v*/*v*) to obtain fifteen fractions (Fr.5.1−Fr.5.15). Fr.5.5 (26.5 mg) was purified by reversed-phase semi-preparative HPLC eluting with CH_3CN−H_2O (40:60) at 6 mL/min to produce **6** (13.9 mg). Fr.6 (185.8 mg) was subjected to Sephadex LH-20 gel CC eluting with CH_2Cl_2−CH_3OH (1:1, *v*/*v*) to afford eleven fractions (Fr.6.1−Fr.6.11). Fr.6.6 (15 mg) was purified by semi-preparative HPLC eluting with CH_3CN−H_2O (35:65) at 4 mL/min to yield **7** (1 mg). Fr.1 (138.1 mg) was subjected to Sephadex LH-20 gel CC eluting with CH_2Cl_2−CH_3OH (1:1, *v*/*v*) to offer twelve fractions (Fr.1.1−Fr.1.12). Fr.1.5 (22.8 mg) was isolated by semi-preparative HPLC eluting with CH_3CN−H_2O (45:55) at 6 mL/min to produce Fr.1.5.1 (4.5 mg), Fr.1.5.1 (4.5 mg) was further purified by semi-preparative HPLC eluting with CH_3CN−H_2O gradient (70:30−100:0, *v*/*v*) at 4 mL/min to obtain **10** (0.9 mg). Fr.1.3 (0.8 mg) was separated by semi-preparative HPLC eluting with CH_3CN−H_2O (50:50) at 6 mL/min to yield **11** (0.4 mg).

The fermented material of Δ*oxaK* deletant strain was extracted with EtOAc (3 × 5 L) to give crude extract (10.7 g), which was performed to silica gel CC eluting with dichloromethane−acetone gradient (100:0−0:100, *v*/*v*) to afford four fractions (Fr.1−Fr.4) based on the HPLC analysis. Fr.3 (166.7 mg) was subjected to Sephadex LH-20 gel CC eluting with CH_2Cl_2−CH_3OH (1:1, *v*/*v*) to give eleven fractions (Fr.3.1−Fr.3.11). Fr.3.4 (32.4 mg) was purified by semi-preparative HPLC eluting with CH_3CN−H_2O (40:60) at 6 mL/min to yield **7** (4.6 mg). Fr.2 (456 mg) was subjected to Sephadex LH-20 gel CC eluting with CH_2Cl_2−CH_3OH (1:1, *v*/*v*) to produce nineteen fractions (Fr.2.1−Fr.2.19). Fr.2.6 (82.8 mg) was isolated by semi-preparative HPLC eluting with CH_3CN−H_2O (40:60) at 4 mL/min to produce Fr.2.6.1, Fr.2.6.1 (30 mg) was further purified by semi-preparative HPLC eluting with CH_3CN−H_2O (30:70) at 4 mL/min to yield **8** (2.8 mg) and **12** (2.5 mg). Fr.4 (87 mg) was subjected to Sephadex LH-20 gel CC eluting with CH_2Cl_2−CH_3OH (1:1, *v*/*v*) to produce nine fractions (Fr.4.1−Fr.4.9). Fr.4.4 (10.3 mg) was separated by semi-preparative HPLC eluting with CH_3CN−H_2O (40:60) at 6 mL/min to give **9** (4.6 mg).

Decaturin H (**10**): pale yellow powder; [α] +140.0 (*c* 0.06, MeOH); UV (MeOH) λ_{max} (log ε): 207 (2.06), 235 (1.98), 271 (0.67), and 334 (0.81) nm; IR (ν_{max}): 3382, 2980, 1700, 1698, 1634, 1566, 1441, 1205, 1137, 1043, 904, 802, and 704 cm^{-1}; CD (MeOH) $\Delta\varepsilon$ (nm): +6.04 (205.5), +5.07 (240.0), +2.33 (240.0), and −0.42 (310.5); ESIMS *m*/*z* 502.3 $[M-H]^-$; HRESIMS *m*/*z* 504.2369 $[M+H]^+$ (Calcd. for $C_{30}H_{34}NO_6$, 504.2381); ^1H and ^{13}C NMR data, see Table S4.

Decaturin I (**11**): pale yellow powder; [α] +275.0 (*c* 0.02, MeOH); UV (MeOH) λ_{max} (log ε): 206 (1.64), 235 (1.44), 271 (0.56), and 334 (0.59) nm; IR (ν_{max}): 3422, 2981, 1717, 1698, 1636, 1565, 1205, 1139, 1043, 906, 802, and 704 cm^{-1}; CD (MeOH) $\Delta\varepsilon$ (nm): +13.89 (210.0), +13.59 (239.0), +6.07 (270.0), and +2.10 (374.0); ESIMS *m*/*z* 518.4 $[M+H]^+$; HRESIMS *m*/*z* 518.2528 $[M+H]^+$ (Calcd. for $C_{31}H_{36}NO_6$, 518.2537); ^1H and ^{13}C NMR data, see Table S4.

Decaturin J (**12**): pale yellow powder; [α] +182.5 (*c* 0.08, MeOH); UV (MeOH) λ_{max} (log ε): 206 (1.58), 233 (1.38), 269 (0.53), and 331 (0.72) nm; IR (ν_{max}): 3357, 1707, 1633, 1567, 1445, 1202, 1137, 1048, 1042, 903, 803, and 704 cm^{-1}; CD (MeOH) $\Delta\varepsilon$ (nm): +0.78 (208.0), +0.51 (270.0), and +0.09 (344.0); ESIMS *m*/*z* 520.2 $[M+H]^+$; HRESIMS *m*/*z* 520.2358 $[M+H]^+$ (Calcd. for $C_{30}H_{34}NO_7$, 520.2335); ^1H and ^{13}C NMR data, see Table S4.

5.12. *Anti-IAV assays*

Compounds **3**−**12** were evaluated for their anti-IAV activities according to the reported procedures[61].

Acknowledgments

This work was supported by grants from the CAMS Innovation Fund for Medical Sciences (CIFMS) (2019-I2M-1-005 and 2021-I2M-1-055), the National Natural Science Foundation of China (No. 31872617 and 82073744), and the central level, scientific research institutes for basic R & D fund business (3332018097). We are grateful to Prof. Yi Tang (Department of Chemical and Biomolecular Engineering, University of California, Los Angeles, CA, USA) for sharing the YET plasmid and the strain *S. cerevisiae* BJ5464. The strain *S. c*. RC01 was kindly provided by Prof. Shushan Gao (Institute of Microbiology, Chinese Academy of Sciences, Beijing, China).

Author contributions

Tao Zhang and Dewu Zhang conceived the study and obtained initial funding. Tao Zhang, Dewu Zhang and Liyan Yu supervised the experiments. Tao Zhang, Guowei Gu and Dewu Zhang conducted experiments. Guodong Liu contributed the strain and the genome of the fungus. Jinxiu Qian and Zhilai Zhan accomplished LC−MS experiments and analysed data. Jinhua Su and Guowei Cai advised on the design and interpretation of data in Figs. 2 and 6. Jianyuan Zhao and Shan Cen performed the anti-IAV activity. Tao Zhang wrote the draft of the manuscript. Tao Zhang, Guowei Gu, Dewu Zhang and Liyan Yu edited the draft of the manuscript. All authors reviewed the final manuscript.

Conflicts of interest

The authors declare no conflicts of interest.

Appendix A. Supporting information

Supporting data to this article can be found online at https://doi.org/10.1016/j.apsb.2022.09.008.

References

1. Matsuda Y, Abe I. Biosynthesis of fungal meroterpenoids. *Nat Prod Rep* 2016;**33**:26−53.
2. Geris R, Simpson TJ. Meroterpenoids produced by fungi. *Nat Prod Rep* 2009;**26**:1063−94.
3. Zhang T, Wan J, Zhan Z, Bai J, Liu B, Hu Y. Activation of an unconventional meroterpenoid gene cluster in *Neosartorya glabra* leads to the production of new berkeleyacetals. *Acta Pharm Sin B* 2018;**8**:478−87.
4. Regueira TB, Kildegaard KR, Hansen BG, Mortensen UH, Hertweck C, Nielsen J. Molecular basis for mycophenolic acid biosynthesis in *Penicillium brevicompactum*. *Appl Environ Microbiol* 2011;**77**:3035−43.
5. Zhao M, Tang Y, Xie J, Zhao Z, Cui H. Meroterpenoids produced by fungi: occurrence, structural diversity, biological activities, and their molecular targets. *Eur J Med Chem* 2021;**209**:112860.
6. Itoh T, Tokunaga K, Matsuda Y, Fujii I, Abe I, Ebizuka Y, et al. Reconstitution of a fungal meroterpenoid biosynthesis reveals the involvement of a novel family of terpene cyclases. *Nat Chem* 2010;**2**:858−64.
7. Barra L, Abe I. Chemistry of fungal meroterpenoid cyclases. *Nat Prod Rep* 2021;**38**:566−85.
8. Mitsuhashi T, Barra L, Powers Z, Kojasoy V, Cheng A, Yang F, et al. Exploiting the potential of meroterpenoid cyclases to expand the chemical space of fungal meroterpenoids. *Angew Chem Int Ed Engl* 2020;**59**:23772−81.
9. Matsuda Y, Awakawa T, Mori T, Abe I. Unusual chemistries in fungal meroterpenoid biosynthesis. *Curr Opin Chem Biol* 2016;**31**:1−7.
10. Lo HC, Entwistle R, Guo CJ, Ahuja M, Szewczyk E, Hung JH, et al. Two separate gene clusters encode the biosynthetic pathway for the meroterpenoids austinol and dehydroaustinol in *Aspergillus nidulans*. *J Am Chem Soc* 2012;**134**:4709−20.
11. Matsuda Y, Awakawa T, Wakimoto T, Abe I. Spiro-ring formation is catalyzed by a multifunctional dioxygenase in austinol biosynthesis. *J Am Chem Soc* 2013;**135**:10962−5.
12. Matsuda Y, Quan Z, Mitsuhashi T, Li C, Abe I. Cytochrome P450 for citreohybridonol synthesis: oxidative derivatization of the and rastin scaffold. *Org Lett* 2016;**18**:296−9.
13. Rojas-Aedo JF, Gil-Durán C, Del-Cid A, Valdés N, Álamos P, Vaca I, et al. The biosynthetic gene cluster for andrastin A in *Penicillium roqueforti*. *Front Microbiol* 2017;**8**:813.
14. Bugni TS, Abbanat D, Bernan VS, Maiese WM, Greenstein M, Van Wagoner RM, et al. Yanuthones: novel metabolites from a marine isolate of *Aspergillus niger*. *J Org Chem* 2000;**65**:7195−200.
15. Holm DK, Petersen LM, Klitgaard A, Knudsen PB, Jarczynska ZD, Nielsen KF, et al. Molecular and chemical characterization of the biosynthesis of the 6-MSA-derived meroterpenoid yanuthone D in *Aspergillus niger*. *Chem Biol* 2014;**21**:519−29.
16. Yaegashi J, Romsdahl J, Chiang YM, Wang CCC. Genome mining and molecular characterization of the biosynthetic gene cluster of a diterpenic meroterpenoid, 15-deoxyoxalicine B, in *Penicillium canescens*. *Chem Sci* 2015;**6**:6537−44.
17. Matsuda Y, Iwabuchi T, Wakimoto T, Awakawa T, Abe I. Uncovering the unusual D-ring construction in terretonin biosynthesis by collaboration of a multifunctional cytochrome P450 and a unique isomerase. *J Am Chem Soc* 2015;**137**:3393−401.
18. Guo CJ, Knox BP, Chiang YM, Lo HC, Sanchez JF, Lee KH, et al. Molecular genetic characterization of a cluster in *A. terreus* for biosynthesis of the meroterpenoid terretonin. *Org Lett* 2012;**14**:5684−7.
19. Matsuda Y, Awakawa T, Itoh T, Wakimoto T, Kushiro T, Fujii I, et al. Terretonin biosynthesis requires methylation as essential step for cyclization. *Chembiochem* 2012;**13**:1738−41.
20. Matsuda Y, Wakimoto T, Mori T, Awakawa T, Abe I. Complete biosynthetic pathway of anditomin: nature's sophisticated synthetic route to a complex fungal meroterpenoid. *J Am Chem Soc* 2014;**136**:15326−36.
21. Rank C, Phipps RK, Harris P, Fristrup P, Larsen TO, Gotfredsen CH. Novofumigatonin, a new orthoester meroterpenoid from *Aspergillus novofumigatus*. *Org Lett* 2008;**10**:401−4.
22. Matsuda Y, Bai T, Phippen CBW, Nødvig CS, Kjærbølling I, Vesth TC, et al. Novofumigatonin biosynthesis involves a non-heme iron-dependent endoperoxide isomerase for orthoester formation. *Nat Commun* 2018;**9**:2587.
23. Mori T, Zhai R, Ushimaru R, Matsuda Y, Abe I. Molecular insights into the endoperoxide formation by Fe(II)/α-KG-dependent oxygenase NvfI. *Nat Commun* 2021;**12**:4417.
24. Matsuda Y, Iwabuchi T, Fujimoto T, Awakawa T, Nakashima Y, Mori T, et al. Discovery of key dioxygenases that diverged the paraherquonin and acetoxydehydroaustin pathways in *Penicillium brasilianum*. *J Am Chem Soc* 2016;**138**:12671−7.
25. Nakashima Y, Mori T, Nakamura H, Awakawa T, Hoshino S, Senda M, et al. Structure function and engineering of multifunctional non-heme iron dependent oxygenases in fungal meroterpenoid biosynthesis. *Nat Commun* 2018;**9**:104.
26. Bai T, Quan Z, Zhai R, Awakawa T, Matsuda Y, Abe I. Elucidation and heterologous reconstitution of chrodrimanin B biosynthesis. *Org Lett* 2018;**20**:7504−8.
27. Tang MC, Zou Y, Watanabe K, Walsh CT, Tang Y. Oxidative cyclization in natural product biosynthesis. *Chem Rev* 2017;**117**:5226−333.
28. Martinez S, Hausinger RP. Catalytic mechanisms of Fe(II)- and 2-oxoglutarate-dependent oxygenases. *J Biol Chem* 2015;**290**:20702−11.
29. Gao SS, Zhang T, Garcia-Borràs M, Hung YS, Billingsley JM, Houk KN, et al. Biosynthesis of heptacyclic duclauxins requires extensive redox modifications of the phenalenone aromatic polyketide. *J Am Chem Soc* 2018;**140**:6991−7.
30. Griffiths S, Mesarich CH, Saccomanno B, Vaisberg A, De Wit PJ, Cox R, et al. Elucidation of cladofulvin biosynthesis reveals a cytochrome P450 monooxygenase required for anthraquinone dimerization. *Proc Natl Acad Sci U S A* 2016;**113**:6851−6.
31. Kato N, Suzuki H, Takagi H, Asami Y, Kakeya H, Uramoto M, et al. Identification of cytochrome P450s required for fumitremorgin biosynthesis in *Aspergillus fumigatus*. *Chembiochem* 2009;**10**:920−8.
32. Hu Y, Dietrich D, Xu W, Patel A, Thuss JA, Wang J, et al. A carbonate-forming Baeyer-Villiger monooxygenase. *Nat Chem Biol* 2014;**10**:552−4.
33. Nakashima Y, Mitsuhashi T, Matsuda Y, Senda M, Sato H, Yamazaki M, et al. Structural and computational bases for dramatic skeletal rearrangement in anditomin biosynthesis. *J Am Chem Soc* 2018;**140**:9743−50.
34. Abe I. Nonheme iron- and 2-oxoglutarate-dependent dioxygenases in fungal meroterpenoid biosynthesis. *Chem Pharm Bull* 2020;**68**:823−31.
35. Macias FA, Carrera C, Galindo JC. Brevianes revisited. *Chem Rev* 2014;**114**:2717−32.
36. Li C, Gloer JB, Wicklow DT, Dowd PF. Antiinsectan decaturin and oxalicine analogues from *Penicillium thiersii*. *J Nat Prod* 2005;**68**:319−22.
37. Zhang Y, Li C, Swenson DC, Gloer JB, Wicklow DT, Dowd PF. Novel antiinsectan oxalicine alkaloids from two undescribed fungicolous *Penicillium* spp. *Org Lett* 2003;**5**:773−6.
38. Dai W, Sandoval IT, Cai S, Smith KA, Delacruz RGC, Boyd KA, et al. Cholinesterase inhibitory arisugacins L-Q from a *Penicillium* sp. isolate obtained through a citizen science initiative and their activities in a phenotype-based zebrafish assay. *J Nat Prod* 2019;**82**:2627−37.
39. Sunazuka T, Omura S. Total synthesis of alpha-pyrone meroterpenoids, novel bioactive microbial metabolites. *Chem Rev* 2005;**105**:4559−80.
40. Li X, Li XM, Zhang P, Wang BG. A new phenolic enamide and a new meroterpenoid from marine alga-derived endophytic fungus *Penicillium oxalicum* EN-290. *J Asian Nat Prod Res* 2015;**17**:1204−12.
41. Zhang P, Li XM, Liu H, Li X, Wang BG. Two new alkaloids from *Penicillium oxalicum* EN-201, an endophytic fungus derived from the marine mangrove plant Rhizophora stylosa. *Phytochemistry Lett* 2015;**13**:160−4.
42. Kitano M, Yamada T, Amagata T, Minoura K, Tanaka R, Numata A. Novel pyridino-α-pyrone sesquiterpene type pileotin produced by a sea urchin-derived *Aspergillus* sp. *Tetrahedron Lett* 2012;**53**:4192−4.

43. Blin K, Medema MH, Kottmann R, Lee SY, Weber T. The antiSMASH database, a comprehensive database of microbial secondary metabolite biosynthetic gene clusters. *Nucleic Acids Res* 2017;**45**:D555−d9.
44. Wang PL, Lib DY, Xie LR, Wu X, Hua HM, Li ZL. Novel decaturin alkaloids from the marine-derived fungus Penicillium oxalicum. *Nat Prod Commun* 2013;**8**:1397−8.
45. Tang MC, Lin HC, Li D, Zou Y, Li J, Xu W, et al. Discovery of unclustered fungal indole diterpene biosynthetic pathways through combinatorial pathway reassembly in engineered yeast. *J Am Chem Soc* 2015;**137**:13724−7.
46. Guengerich FP. Mechanisms of cytochrome P450-catalyzed oxidations. *ACS Catal* 2018;**8**:10964−76.
47. Denisov IG, Makris TM, Sligar SG, Schlichting I. Structure and chemistry of cytochrome P450. *Chem Rev* 2005;**105**:2253−77.
48. Ortiz de Montellano PR. Hydrocarbon hydroxylation by cytochrome P450 enzymes. *Chem Rev* 2010;**110**:932−48.
49. Bai J, Yan D, Zhang T, Guo Y, Liu Y, Zou Y, et al. A cascade of redox reactions generates complexity in the biosynthesis of the protein phosphatase-2 inhibitor rubratoxin A. *Angew Chem Int Ed Engl* 2017;**56**:4782−6.
50. Zhang DW, Zhao JY, Zhou JQ, Wei T, Yu LY. Antiviral chemical constituents from the fungus *Penicillium* sp. CPCC 400786. *Mycosystema* 2020;**39**:434−40.
51. Li L, Tang MC, Tang S, Gao S, Soliman S, Hang L, et al. Genome mining and assembly-line biosynthesis of the UCS1025A pyrrolizidinone family of fungal alkaloids. *J Am Chem Soc* 2018;**140**:2067−71.
52. Lin HC, Tsunematsu Y, Dhingra S, Xu W, Fukutomi M, Chooi YH, et al. Generation of complexity in fungal terpene biosynthesis: discovery of a multifunctional cytochrome P450 in the fumagillin pathway. *J Am Chem Soc* 2014;**136**:4426−36.
53. Barriuso J, Nguyen DT, Li JW, Roberts JN, MacNevin G, Chaytor JL, et al. Double oxidation of the cyclic nonaketide dihydromonacolin L to monacolin J by a single cytochrome P450 monooxygenase. *LovA. J Am Chem Soc* 2011;**133**:8078−81.
54. Mizutani M, Stao F. Unusual P450 reactions in plant secondary metabolism. *Arch Biochem Biophys* 2011;**507**:194−203.
55. Yamamoto H, Katano N, Ooi A, Inoue K. Secologanin synthase which catalyzes the oxidative cleavage of loganin into secologanin is a cytochrome P458. *Phytochemistry* 2000;**53**:7−12.
56. Chooi YH, Hong YJ, Cacho RA, Tantillo DJ, Tang Y. A cytochrome P450 serves as an unexpected terpene cyclase during fungal meroterpenoid biosynthesis. *J Am Chem Soc* 2013;**135**:16805−8.
57. Wu B, Ohlendorf B, Oesker V, Wiese J, Malien S, Schmaljohann R, et al. Acetylcholinesterase inhibitors from a marine fungus *Talaromyces* sp. strain LF458. *Mar Biotechnol* 2015;**17**:110−9.
58. Podust LM, Sherman DH. Diversity of P450 enzymes in the biosynthesis of natural products. *Nat Prod Rep* 2012;**29**:1251−66.
59. Ding B, Wang Z, Huang X, Liu Y, Chen W, She Z. Bioactive alpha-pyrone meroterpenoids from mangrove endophytic fungus *Penicillium* sp. *Nat Prod Res* 2016;**30**:2805−12.
60. Zhang T, Ren P, Chaturvedi V, Chaturvedi S. Development of an Agrobacterium-mediated transformation system for the cold-adapted fungi *Pseudogymnoascus destructans* and *P. pannorum*. *Fungal Genet Biol* 2015;**81**:73−81.
61. Gao Q, Wang Z, Liu Z, Li X, Zhang Y, Zhang Z, et al. A cell-based high-throughput approach to identify inhibitors of influenza A virus. *Acta Pharm Sin B* 2014;**4**:301−6.